Storm-induced precipitation variability control of long-term erosion

E. Gayer, Laurent Michon, P. Louvat, J. Gaillardet

Storm-induced precipitation variability control of long-term erosion

E. Gayer [a,*], L. Michon [b], P.Louvat [a], J. Gaillardet [a]

[a] Institut de Physique du Globe de Paris, Sorbonne Paris Cité, Université Paris Diderot, UMR 7154 CNRS, F-75005, Paris, France
[b] Laboratoire GéoSciences Réunion, Université de La Réunion, Institut de Physique du Globe de Paris, Sorbonne Paris Cité, UMR 7154 CNRS, F-97744 Saint Denis, France

A B S T R A C T

Erosion is often treated as a continuous process, yet it occurs through discrete events such as floods and landslides of variable magnitude and periodicity. It has also long been expected to be strongly dependent on precipitation, however, the influence of temporal rainfall variability upon long-term evolution of landscapes remains unclear. Here we report high erosion rates (0.8 to ~10 mm yr^{-1} over ~70 ka) estimated from paleovolcanic reconstructions across a steep rainfall gradient on Reunion Island, which show that long-term erosion rates are influenced by the cyclone-induced variability of precipitation. Geostatistical analysis of 30 years of daily rainfall records reveals that erosion rates are high where the local climate is the driest and where the difference in intensity between extreme rainfall events and prevailing precipitation is the strongest. This implies that the intrinsic variability of precipitation impacts landscape evolution not only through extreme meteorological events, but also through background rainfall-induced parameters such as humidity and dryness, which modulate the erosion threshold of the Earth's Critical Zone.

1. Introduction

Erosion plays a key role in the feedback between topography, tectonics and climate (Steer et al., 2014; Willett, 1999), and regulates Earth's habitability through its effect on the global CO_2 budget (Stallard, 1998), soil formation (Brantley et al., 2007) and sediment transport (Hilton et al., 2008). Erosion is broadly expected to be dependent on mean precipitation rates (Ferrier et al., 2013a, 2013b; Reiners et al., 2003) but the impact of climate variability (Tucker and Bras, 2000), as opposed to mean climate, has long been suggested, and recently examined (e.g. via discharge variability; DiBiase and Whipple, 2011; Scherler et al., 2017). However, important components of how short-term precipitation events influence long-term erosion remain unknown.

Rainfall variability is often heavily influenced by short-term extreme precipitation events. In the tropics, such extreme rainfall episodes are amongst the most hazardous and damaging of natural disasters (Garcin et al., 2005; Nott, 2007). Cyclones are known to trigger catastrophic erosional events and floods, which result in a massive transport of sediments to the ocean. Several studies have investigated cyclone-induced short-term erosion rates using the sediment budget of single storm events (Allemand et al., 2014; Dadson et al., 2003; Hartshorn et al., 2002; Reid and Page, 2003), but limited studies have explored the role of extreme storms and engendered precipitation variability on the long-term evolution of landscapes (e.g. DiBiase and Whipple, 2011; Scherler et al., 2017).

Volcanic islands often present high elevated and dramatically escarped landforms due to high erosion rates (Ferrier et al., 2013b; Hildenbrand et al., 2008; Louvat and Allègre, 1997). Such elevated relief, compared to the surrounding flat ocean, affect local atmospheric circulation and typically create large variation in climate, particularly in precipitation. In addition, volcanic islands represent transient landscapes with no tectonic deformation (compared to continental settings where erosion is counterbalanced by uplift). Such features make volcanic islands natural laboratories to study the effect of climate on erosion and have been particularly used to investigate the influence of mean annual precipitation rates on river incision and on bedrock erodibility (Ferrier et al., 2013a; Murphy et al., 2016).

In this study we use Reunion Island (Indian Ocean), one of the wettest places on Earth, to examine not only the effect of the precipitation background regime on erosion but also the influence of the storm-induced precipitation variability on long-term erosion rates. As a volcanic tropical island, Reunion shows a great contrast in precipitation between its windward and leeward sides with annual rainfall rates ranging from 11 $m yr^{-1}$ to 0.5 $m yr^{-1}$, respectively. In addition, Reunion is subjected to intense and destructive storms during the rainy season, which equivalently touch

* Corresponding author.
E-mail address: egayer@ipgp.fr (E. Gayer).

both of its sides and are responsible for a strong seasonality in annual precipitation. Since 1964, tropical cyclones have occurred approximately every 3 years and many of them hold the rainfall world records (e.g. 3.9 m in 72 h during cyclone Gamède in 2007; Quetelard et al., 2009). With minimal variation in lithology, an exceptionally wide range of precipitation rates and the occurrence of intense tropical storms, Reunion is ideal to study the effects of extreme contrasts in precipitation regimes on erosion. These extreme climatic conditions give rise to particularly rapid landscape evolution, notably through landslides and massive sediment transfer (Garcin et al., 2005; Saint-Ange et al., 2011). Here we present new erosion rates on Reunion, derived from the volume of material removed from watersheds since the formation of the latest volcano surfaces, that we use to investigate the influence of precipitation variability on long-term erosion over millennial timescale.

In the following, we first introduce the study site and summarize the volcanic history of Reunion. Then, we describe the method we used to estimate the erosion rates of the seven largest watersheds of Reunion from initial topography reconstruction techniques. Next, we present an analysis of the precipitation records over the island and, finally, we discuss the influence of topography and of climatic variability on erosion intensity.

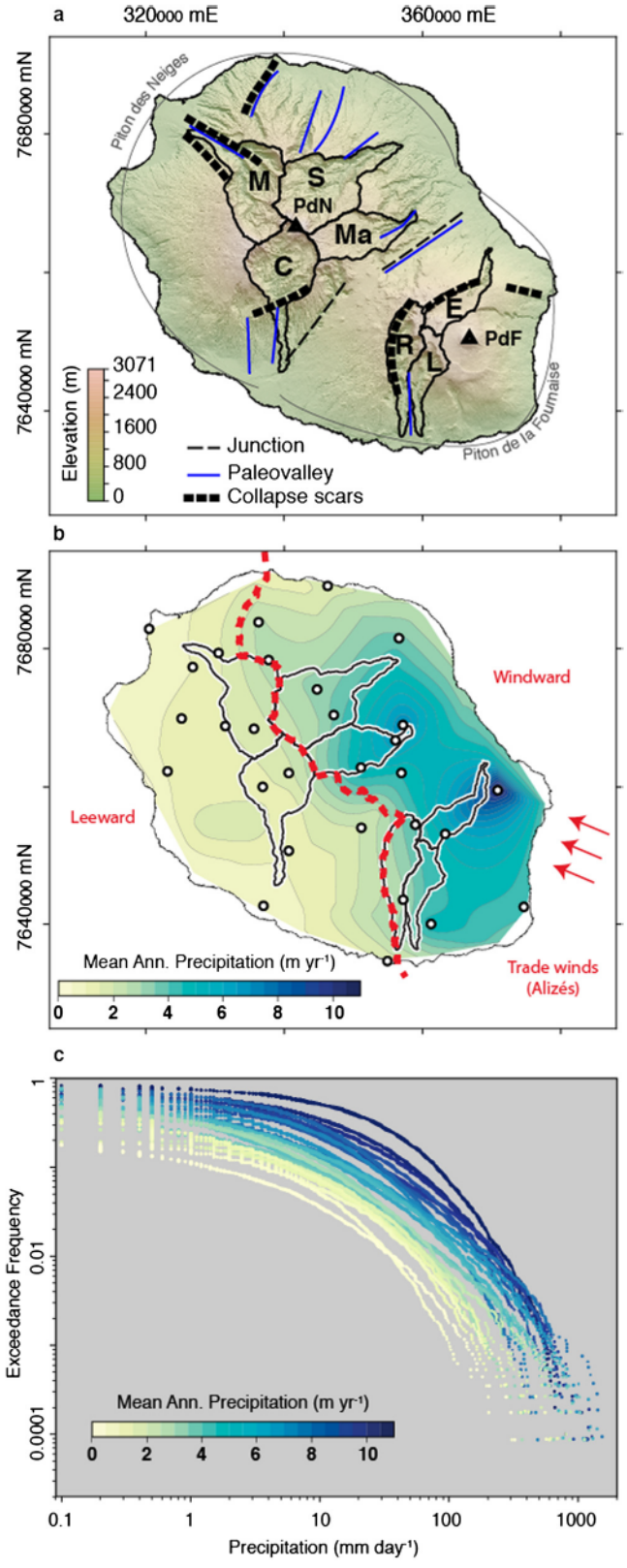

2. Geological settings

Located in the western Indian Ocean, Reunion Island exhibits an elliptical shape due to the juxtaposition of the two basaltic shield volcanoes, the dormant Piton des Neiges (PdN, 3,071 mamsl) and active Piton de la Fournaise (PdF, 2,632 mamsl; Fig. 1a). The current massif of PdN results from the accumulation of basaltic lava flows between >2.1 Ma and 430 ka, followed by trachybasaltic flows between 350 and 70 ka. Like all volcanoes, PdN had periods of edifice construction and periods of quiescence during which erosion dismantled parts of the massif (Salvany et al., 2012). The two most recent edifices of PdN are PdN3 and PdN4 (stages 3 and 4 in Salvany et al. (2012)'s volcanostratigraphy), built between ~350 and 210 ka, and between 140 and 70 ka, respectively. PdN3 is a large symmetrical stratovolcano of ~3700 m high that has been dissected by erosion after a period of ignimbritic eruptions at 180 ka (Salvany et al., 2012). Erosion of PdN3 resulted in topographical depressions that were subsequently filled when lava flow emission resumed around 140 ka to build PdN4 until 70 ka. This new edifice only partly filled the depressions incised in PdN3 as shown by the well-preserved paleosurfaces East and North of PdN's summit (Marsouins, Belouve) and by the perched lava flows at the outlet of the cirque of Cilaos in the South (Fig. S1a). Although remnants of this PdN4 edifice have not yet been reported on its northwestern part, the eastern limit of the cirque of Mafate partly coincides to lava flows belonging to PdN4. Since 70 ka, the activity of PdN drastically declined with only a few sporadic explosive eruptions reported around 30 ka (Salvany et al., 2012).

The PdF volcano is younger than PdN and built on its eastern flank since at least 530 ka, with the superposition of trachybasaltic (530 to 400 ka) followed by basaltic lava flows (Gillot et al., 1994; Michon et al., 2016). Geological data and isotopic ages suggest that PdF experienced several collapse events that contributed to periods of volcano dismantling. At around 80 ka, the collapse of the Morne Langevin caldera (Fig. 2a) disconnected the southwest-

Fig. 1. Map of Reunion Island and precipitations rates. (**a**) Topography of Reunion derived from 25 m digital elevation model (DEM) and location of the two volcanoes Piton des Neiges (PdN) and Piton de la Fournaise (PdF) and of the seven studied drainage areas: cirques of Cilaos (C), Mafate (M), Salazie (S), Marsouins (Ma) and Est River (E), Langevin (L) and Remparts canyons (R). The thin black dashed lines represent the junction between the two volcanoes and the thick black dashed lines represent collapse landslides scars. Blue lines account for the locations of paleovalleys observed in the field, that were incised during periods of quiescence and later filled by lava flows while the lava emission was renewing. (**b**) Mean annual precipitation from 1981 to 2010 resampled to 25 m resolution (Météo France). Locations of rain gauge stations are shown as white circles. Red arrows represent the prevailing pattern of easterly surface winds called *Alizés*. (**c**) Exceedance frequency plots for daily precipitation. Curves are colored following the mean annual precipitation rates at each rain gauge station. (For interpretation of the colors in the figure(s), the reader is referred to the web version of this article.)

ern flank of PdF from lava flow emission, enabling the incision of the Remparts paleovalley (Mairine and Bachèlery, 1997). Magma overflowing from the Morne Langevin caldera led to a partial filling of the paleovalley until around 60 ka (Michon et al., 2016). Erosion then incised the paleosurfaces of the southwestern and northern flanks to shape the present-day Remparts, Langevin and Est canyons (Fig. 1a).

Both edifices, PdN and PdF, present hydrothermal weathering close to their centers and both volcanoes have experienced, during their evolution, multi-directional flank landslides leading to the intercalations of debris avalanche deposits within the piles of lava flows (Figs. 1a, and S2, Michon et al., 2016; Oehler et al., 2008). Nonetheless at the island scale, both massifs present a similar lithological distribution and both present a similar evolution with succession of edification periods followed by dismantling periods (Gillot et al., 1994; Michon et al., 2016; Oehler et al., 2008; Salvany et al., 2012).

The relief resulting from the juxtaposition of the two volcanoes forms an efficient barrier to the East trade winds, leading to an exceptional gradient in mean annual precipitation rates (Fig. 1b) and making Reunion one of the wettest places on Earth. Between 1981 and 2010, precipitation rates averaged 11 $m\,yr^{-1}$ on the wet windward northeastern side of the island, which hosts a lush rainforest (Strasberg et al., 2005). In contrast, precipitation rates of only 0.5 $m\,yr^{-1}$ are recorded on the leeward southwestern side where rain shadow aridity prevails (Fig. 1b). The watersheds under investigation for erosion rates evaluation are located on both volcanoes and both sides of the island (Fig. 1) and represent the 7 largest basins of Reunion.

3. Methods

In order to estimate basin-averaged long-term erosion rates across Reunion, we used a common method that consists of calculating the volume of eroded material over a time period between the construction of a pre-erosional topography and the present (Hildenbrand et al., 2008; Salvany et al., 2012). Such a method is particularly well suited for Reunion Island since remnants of the surfaces of the two volcanoes are present at the multimillennial timescale. However, application of this approach to watersheds with consecutive episodes of filling and erosion can lead to underestimation of the resulting erosion rates when not considering the youngest pre-erosional topography. For example, models based on the PdN3 initial topography and the present-day PdN's watersheds topographies (Salvany et al., 2012) have excluded the building of PdN4 in the paleodepressions incised in PdN3. Consequently, the actual erosion rates since PdN3 construction (180 ka in Salvany et al., 2012) have been underestimated. To prevent this issue, we targeted (i) the watersheds, which have been only eroded during the last period of quiescence of PdN (post PdN4, i.e. since ~70 ka; Cilaos, Mafate, Salazie and Marsouins, Fig. 1a) and (ii) watersheds undisturbed by the recent PdF activity over the same period of time (since ~60 ka; Remparts, Langevin and Est canyons, Fig. 1a). Thus, we quantify the volume of eroded material based on the reconstruction of the 72 ± 3-ka-old PdN volcanic paleotopography (PdN4) and the 63 ± 3-ka-old paleosurfaces of PdF. Constraints for these reconstructions are published K-Ar ages (Gillot et al., 1994; Salvany et al., 2012) of well-preserved primary volcanic landforms, as well as geomorphological, geological and field observations (Fig. 2a). Assuming that the drainage divides have remained unchanged relative to the incision of the studied drainage areas (on the ~70 ka timescale), and using a 25 m digital elevation model (DEM; resampled from the 5 m DEM produced by the Institut Géographique National – IGN), we digitized elevations at over 8,000 points on the uneroded remnants of the volcanoes in order to interpolate pre-erosional surfaces between them. Two different methods were used to approximate the geometry of the paleosurfaces of the ~60 ka PdF and the ~70 ka PdN.

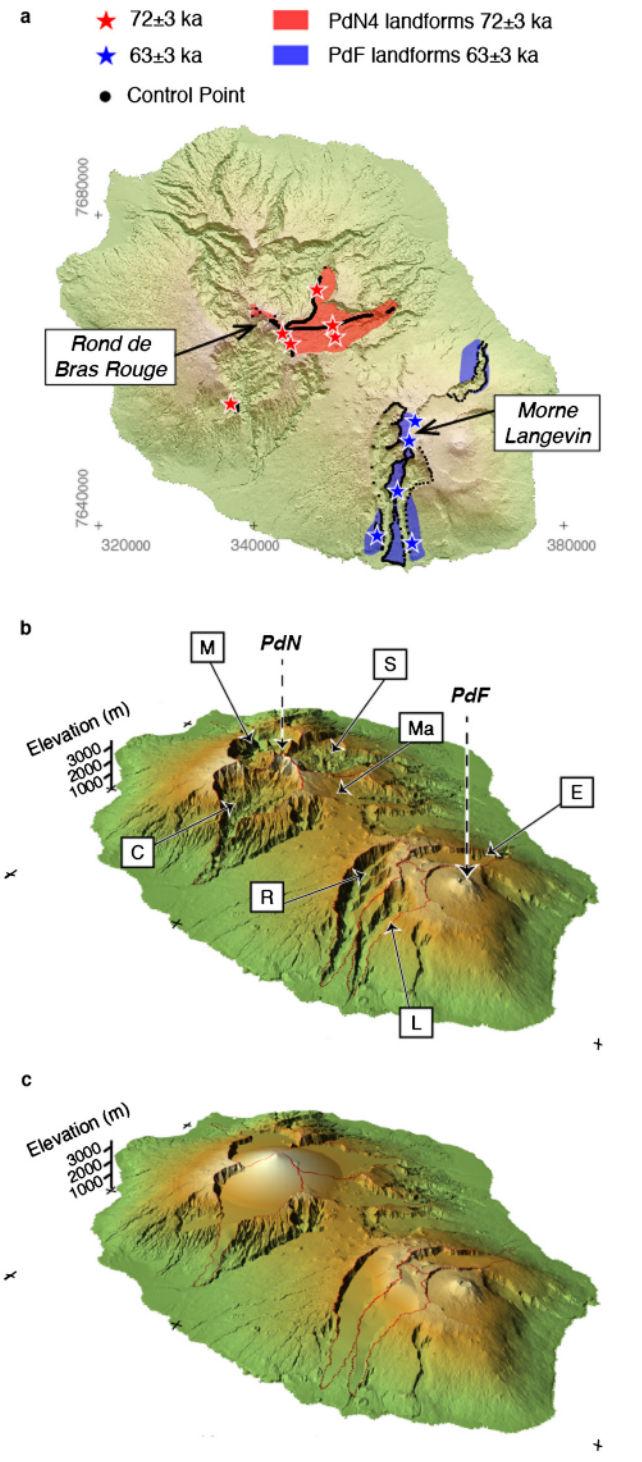

Fig. 2. Geomorphic reconstruction of Piton des Neiges and Piton de la Fournaise. (**a**) K-Ar ages of primary volcanic landforms (stars, Gillot et al., 1994; Salvany et al., 2012). The 72 ± 3 ka dated remnant surfaces are indicated in red, the 63 ± 3 ka dated remnant surfaces are indicated in blue. The remnants used to reconstruct the pre-eroded paleosurfaces are indicated in black (control point). (**b**) 3D representation of the current 25 m DEM (UTM projection Zone 40S). Cirques of Cilaos (C), Mafate (M), Salazie (S), Marsouins (Ma) and Est River (E), Langevin (L) and Remparts canyons (R). (**c**) 3D representation of the reconstructed PdN4 (72 ± 3-ka-old paleoedifice, right circular cone model: *CD* model) and of the PdF 63 ± 3-ka-old paleosurfaces.

3.1. Paleotopography reconstruction over the PdF's basins

For each basin of PdF, the pre-erosional topographies were reconstructed by fitting a surface to the interfluve remnants (control points) of the 63 ± 3-ka-old southern and northeastern flanks of the volcano, using a natural neighbor interpolation technique (Fig. 2c, Sibson, 1981). Uncertainties in such reconstructions are difficult to assess since they are based on field observations, and would need uncertainties in parameters such as drainage area or in the probable erosion of the interfluve remnants. With an interfluve surface erosion rate slower than 0.1 mmyr^{-1} over the last ~60 ka on the PdF southern flank (Sarda et al., 1993), uncertainties in eroded volume in the PdF watersheds could be assumed negligible relative to the uncertainties in bedrock ages. However, to evaluate the sensitivity of our method and the errors in the calculated volume of eroded material, we tested a basis spline interpolation technique (instead of natural neighbor) on fewer control points for the Remparts and the Langevin basins. Volumes calculated from this altered model (since it does not consider all the control points we observe) differ from our estimates by 5% for Remparts and by 20% for Langevin. Therefore, we decided to use the upper value of 20% as uncertainties in the calculated volumes of eroded material for the three PdF's basins.

3.2. PdN's paleoedifice reconstruction

The basin perimeter fitting method could not be used to approximate paleosurfaces across the PdN's watersheds due to their significant width (up to 10 km wide each). Instead, we reconstructed PdN4 at 72 ± 3 ka ago, from the shape and the K-Ar ages (Gillot et al., 1994; Salvany et al., 2012) of its very well preserved eastern flank (Marsouins surface, Belouve surface; Figs. 2a, 2b, S1a, S3a, S3b and S3c) as well as of scattered remnants of the volcano topography (Figs. 2a, S1a).

We developed a new approach to reconstruct PdN's initial topographies at different stages of growth based on its conic shape (Salvany et al., 2012), and on the remarkable symmetry of the geometrical form of many volcanic edifices (i.e. right circular cones or curved cones, e.g. Mayon-Philippines, Etna-Italy, Fuji-Japan). Our method consists in three steps. (i) The first step identifies the center of the volcano we seek to reconstruct using the location and elevation of uneroded remnants (control points). (ii) The second step uses the resulting center along with the location and elevation of the same uneroded remnants to estimate the general shape of the volcano flanks (i.e. straight line or curved line). (iii) Finally, from this general shape, the third step consists in modeling a surface that best fit the location and elevation of the uneroded remnants (i.e. right circular cone or curved cone). We validated this approach by comparing our model of the PdN3 volcano (~210 ka PdN) to the previous study by Salvany et al. (2012), and then we used our method to generate two models of the PdN4 in order to best estimate the volumes of eroded material over the Cilaos, Mafate, Salazie and Marsouins watersheds.

PdN3 edifice is particularly well preserved over the island with large remnant areas on its western and northern side (Fig. S1a). First, we used over 10,000 control points on the western and northern remnant flanks of PdN3 (Fig. S1a) to estimate its crater central position in two different ways: (i) by finding the center of a right circular cone that best fits the control points (*CD* method), and (ii) by finding the best Spearman correlation (Well and Myers, 2002) between all the control points (*Sp* method). Both methods provide very close centers located in Rond du Bras Rouge (Figs. S1a, S3a, S3b, and S3c), in good agreement with the position of the central crater estimated from the distribution of dykes observed in the Cilaos, Mafate and Salazie cirques (Chaput et al., 2014; Chevallier and Vatin-Perignon, 1982). Using each crater central position, we then determined the general shape of PdN3 by plotting the distance between the center and each control points against their elevation (Figs. S1b, S1c). With both center locations, PdN3 shows a conical shape that we modeled as a right circular cone that best fits the uneroded remnants. These two models (with the two different crater center locations) of PdN3 initial topography are in good agreement with the model of Salvany et al. (2012) with similar center locations, similar shapes and similar summit elevations (3,562 m and 3,507 m for our two models vs. 3,700 m for Salvany's model).

To reconstruct the PdN4's initial topography, we reproduced the same method, but using the locations and elevations of control points on the 72 ± 3 ka remnants surfaces (Marsouins and Belouve, Figs. 2a, S1a, S3a, S3b, and S3c) and of scattered remnants. First, we determined two crater centers (with both *CD* and *Sp* methods) located in Rond de Bras Rouge (Fig. S1a) and less than 1 km apart from the centers of PdN3. Assuming that the volcano center did not significantly change with time, we used the average location between the PdN3 and PdN4 centers from each *CD* and *Sp* methods (Fig. S1a) to deduce the general shape of the volcano. Unlike for PdN3, the control points show a general shape with a concave flank profile for PdN4 (Figs. S1d, S1e), which can be explained by the emission of a higher proportion of silicic lava flows (Kluska, 1997) in the preexisting paleocirques. In order to test the sensitivity of our method and because a concave profile can be fitted in several ways, we generated two different models for PdN4 based on two different flank shape fitting techniques. In the first model (called *CD* model), we used the center determined from the *CD* method and we approximated the shape of the volcano as a pile of two right circular cones to best fit the uneroded remnants (Fig. S1d). In the second model (called *Sp* model, Fig. S1e), we used the center determined by the *Sp* method and fitted the flank shape with a logarithmic curve, $h = m \times \log(r) + c$, where r is the radius of the volcano base, h is the height of the volcano, m and c are constants (with m a negative number) following the study of Francis and Abbot (1973). However, when using the *Sp* model, a maximum elevation needs to be assumed. Here, we suggest a maximum elevation of 3,500 ± 200 m based on the ~3,500 m maximum elevation given by the *CD* model, the ~3,500 m summit of our two PdN3 models and based on the 3,700 m maximum elevation estimated for PdN3 by Salvany et al. (2012). Noteworthily, varying this maximum elevation by 200 m (3,500 ± 200 m), the volume of eroded material only changes by less than 1% showing that the choice of a maximum elevation of 3,500 m has insignificant effects on the calculated eroded volumes and inferred erosion rates.

Finally, uncertainties on our models were generated using the two-sigma error given by the methods we used to best fit the curved flank profile of PdN4. For the *CD* model that represents the initial topography of PdN4 as a pile of 2 right circular cones, we generated a surface two-sigma higher in elevation than the best fit model and another surface two-sigma lower, representing the maximal and minimal bounds of the *CD* model, respectively (Fig. S1d). We generated the same upper and lower bounds for the *Sp* model (Fig. S1e) and used them to estimate the uncertainties on the eroded volumes.

3.3. Eroded volume and erosion rates calculation

On the one hand, for all the PdF's basins, we calculated the volumes of eroded material by multiplying the DEM cell size of 25 m by the difference between modern and initial topography elevations (Fig. 2c). Then the basin-averaged erosion rates were determined by dividing the volume of material eroded in the different basins by their drainage area (calculated using a steepest gradient flow algorithm on the 25 m DEM) and by the age of the reconstructed paleosurfaces (63 ± 3 ka; age, bedrock density, and

Table 1
Eroded volumes and erosion rates. For the watersheds of PdN, eroded volumes were derived by averaging the volumes estimated with both the *CD* and *Sp* initial topography models (cf. section 3.3). As an example, for Salazie basin, the *CD* and *Sp* models give volumes of eroded material of 70.0 ± 10.1 and 59.6 ± 5.4 km^3, respectively (where errors are estimated from the upper and lower bounds of each model, cf. section 3.3). An averaged volume of 64.8 ± 5.7 km^3 was then used to calculate the erosion rates of this watershed. Basin-averaged erosion rates are derived from the volumes of material eroded using rock density of 2.85 ± 0.15 g cm^{-3}.

	Area (km^2)	Eroded volume (km^3)	Bedrock age (ka)	Erosion rate (t km^{-2} yr^{-1})	Erosion rate (mm yr^{-1})
Cilaos	100	71.8 ± 3.6	72 ± 3	28355 ± 1716	9.9 ± 0.5
Salazie	121	64.8 ± 5.7	72 ± 3	21192 ± 2129	7.4 ± 0.7
Mafate	108	55.7 ± 5.1	72 ± 3	20430 ± 2122	7.2 ± 0.7
Remparts	59	17.6 ± 3.5	63 ± 3	13550 ± 2876	4.8 ± 1.0
Est	40	8.1 ± 1.6	63 ± 3	9210 ± 1955	3.2 ± 0.7
Langevin	40	8.3 ± 1.7	63 ± 3	9370 ± 1988	3.3 ± 0.7
Marsouins	69	3.9 ± 1.6	72 ± 3	2223 ± 956	0.8 ± 0.3

eroded volume uncertainties were propagated through the erosion rate calculations).

On the other hand, for each PdN basin, two different sets of volumes were calculated by subtracting the modern topography of the watersheds to the PdN4's initial topography from *CD* model and to the PdN4's initial topography from *Sp* model. In addition, by subtracting the modern topography of the basin to the upper and lower bounds of the *CD* and *Sp* models, we estimated uncertainties on the eroded volume for each PdN basin and each model. Finally, because none of the initial topography from the *CD* or *Sp* models could be chosen over the other, the eroded volumes of each watershed were calculated averaging the corresponding eroded volume resulting from each model. Basin-averaged erosion rates were then calculated by dividing the resulting eroded volume by the watershed drainage area and by the age of PdN4 (72 ± 3 ka).

3.4. Climate data analysis

To evaluate the climatic control on erosion in Reunion, we compiled 30 years (1981–2010) of daily precipitations on 29 rain gauge stations from Météo France (Météo France, French national meteorological agency). Mean annual precipitation rates were derived from the daily precipitation rates over these gauges and used to estimate basin-averaged mean annual precipitation rates. In addition to background precipitation regime, we examined the extreme precipitation events using the 11 storms of Tropical to Very-Intense-Tropical Cyclone Class that hit Reunion between 1981 and 2010, investigating their trajectories and induced rainfall intensities. Such extreme events being responsible for fluctuations in the precipitation regime, a rainfall variability analysis across Reunion was also conducted by calculating (i) the coefficient of variation of daily precipitation, CV-p, defined as standard deviation of daily precipitation divided by mean daily precipitation, as well as (ii) the annual CV-p corresponding to the annual coefficient of variation of daily precipitation for each year between 1981 and 2010 and for each rain gauge station.

4. Results: Reunion Island a hotspot of erosion on Earth

The calculated volumes of eroded material for each of the 7 studied watersheds range from 71.8 ± 3.6 to 3.8 ± 1.6 km^3 for the Cilaos and Marsouins basins respectively (Table 1). Over the last ~70 ka, we estimated that the 7 largest watersheds of Reunion supplied a total of 230 km^3 of sediment to the ocean, corresponding to 10% of the emerged volume of the island.

The calculated volumes of eroded material, inferred from paleotopography reconstructions, are consistent with the presence of vast off-shore volcaniclastic deep-sea fans around Reunion (Mazuel et al., 2016; Saint-Ange et al., 2011; Sisavath et al., 2012). In particular, our estimated volume of 71.8 ± 3.6 km^3 eroded from the Cilaos basin (Fig. 1a) since PdN4 matches the ~75 km^3 of the most superficial volcaniclastic depositional unit observed over the Cilaos deep-sea fan (Sisavath et al., 2012). This volume of sediment in the Cilaos fan was estimated by multiplying the fan area of 15,000 km^2 by the thickness of the most superficial volcaniclastic depositional unit (~5 m, corresponding to the last turbidite activity <80 ka; Sisavath et al., 2012).

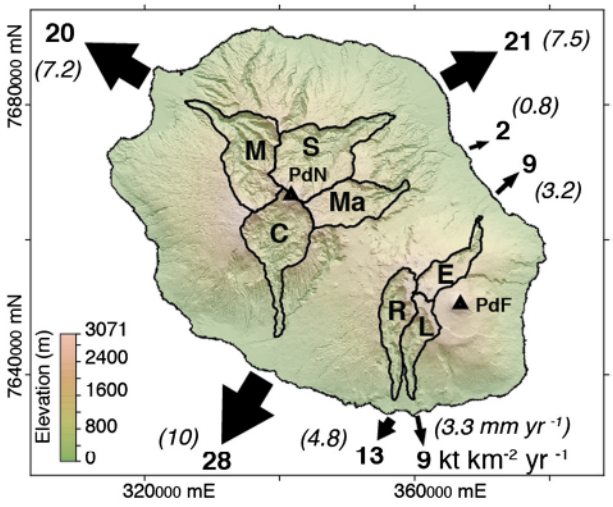

Fig. 3. Erosion rates across Reunion Island. Erosion rates in Reunion calculated from topographical reconstructions of the 72 ± 3-ka-old PdN and 63 ± 3-ka-old PdF paleosurfaces. Black arrows indicate mean annual fluxes (in kt km^{-2} yr^{-1}) of eroded material from the 7 major watersheds of Reunion, delimited with black lines. Erosion rates (in mm yr^{-1}) are indicated in parentheses.

Long-term basin-averaged erosion rates were derived from the calculated volumes of eroded material and the ages of the paleovolcanic surfaces, for each of the 7 studied watersheds. Resulting rates range from 0.8 ± 0.3 mm yr^{-1} for Marsouins to almost 10 mm yr^{-1} (9.9 ± 0.5 mm yr^{-1}) for Cilaos (the basins with the best constraints on PdN4 reconstructions, Fig. 3, Table 1). These values exceed most of those reported for other volcanic islands (Ferrier et al., 2013b; Gayer et al., 2008; Hildenbrand et al., 2008) and make Reunion a hotspot of erosion on Earth (Louvat and Allègre, 1997). In contrast to active orogens, where similar values have been reported (Dadson et al., 2003; Larsen et al., 2014), these high erosion rates cannot be related to tectonic activity, as Reunion presents neither uplift, nor significant subsidence (Gallart et al., 1999) and only minor microseismicity (Michon et al., 2015).

5. Discussion

5.1. Climatic control on intense erosion rates

Such a wide range of erosion rates, over one order of magnitude (Fig. 3) across a small and tectonically inactive island pro-

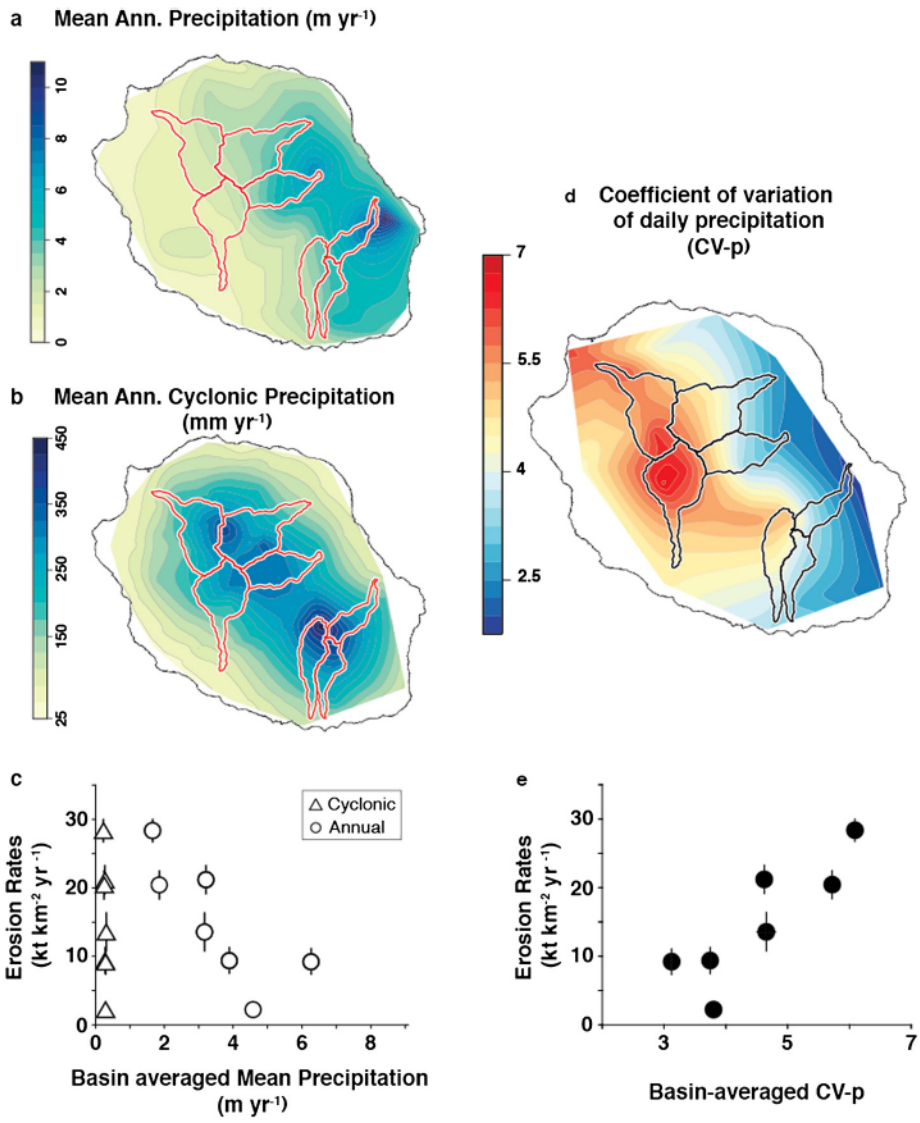

Fig. 4. Precipitation regimes, precipitation variability, and erosion across Reunion. (**a**) Mean annual precipitation from 1981 to 2010 (Météo France) resampled to 25 m resolution. (**b**) Mean annual cyclonic precipitation resampled to 25 m resolution for the period 1981–2010 (scale is different from **a**). (**c**) Relationship between basin-averaged erosion rates and 1) upstream-averaged mean annual precipitation rates (circles); 2) upstream-averaged mean annual cyclonic precipitation rates (triangles), displaying no major gradient across the 7 watersheds. (**d**) Spatial distribution of the coefficient of variation of daily precipitation over Reunion (CV-p), calculated from 30 years record of daily precipitation rates over 29 rain gauge stations across the island. (**e**) Basin-averaged erosion rates as a function of CV-p.

vides an opportunity to evaluate climatic and topographic controls on erosion. Surprisingly, we found that basin-averaged erosion rates are inversely correlated with mean annual precipitation rates ($r^2 = 0.6$; Fig. 4c), which is inconsistent with the general assumption of increasing erosion rates as a function of higher precipitation rates and contrasts with previous observations on other volcanic islands (e.g. Ferrier et al., 2013b) and in continental mountainous settings (e.g. Moon et al., 2011). The disadvantage of testing mean annual precipitation rates is that they average daily rainfall amounts that can vary greatly: from days without rain to extreme rainfall events which are capable of triggering landslides and are responsible for intense water discharge. Over the last 30 years, 11 storms of Tropical to Very-Intense-Tropical Cyclone Class have hit Reunion with diverse trajectories (Fig. S4). We used these extreme events, to model the spatial distribution of the mean annual cyclonic precipitation rates (or Cyclonic Precipitation Regime) in Reunion (Fig. 4b) in order to evaluate their effect on erosion. The pattern shows a maximum rainfall zone centered on the summits that contrasts with the mean annual total precipitation spatial distribution (or Total Precipitation Regime). Such a difference results from a seasonal change in the mean elevation of the temperature inversion layer, in which the atmospheric temperature increases with altitude. In Reunion, during two-thirds of the year (winter-centered), the inversion layer is low (between 2000 and 2500 m, Barcelo and Coudray, 1996; Réchou et al., 2014) and acts as a cap on the upward movement of air, restricting rainfall to low elevations and inducing maximum precipitation on the wet windward flank of the island (Fig. 4a). On the contrary, during austral summer, a high elevation or even absence of the temperature inversion layer (Barcelo and Coudray, 1996; Réchou et al., 2014) allows the tropical depression to cause heavy rains near the summits and on both wet windward and dry leeward sides of the island (Fig. 4b). From this pattern of extreme events, which presents no gradient of intensity across the island, we find no significant correlation between the erosion rates and the Cyclonic Precipitation Regime (Fig. 4c). These results suggest that neither the absolute intensities of extreme precipitation events nor the mean annual precipitation rates exert a positive feedback on long-term erosion.

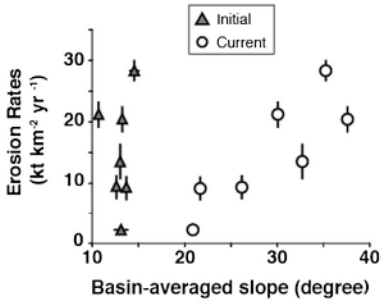

Fig. 5. Relationships between erosion rates and topography gradient across Reunion. Triangles show the initial basin-averaged slope of the 7 studied watersheds. Averaged slopes are calculated by averaging the slopes of the initial topography reconstructed for the 7 basins. Circles represent the current basin-averaged slope of the same 7 watersheds. Present day basins-averaged slopes differ from one basin to another and are correlated with the long-term erosion rates while initial slopes are similar for the 7 basins. This indicates that slopes evolved as erosion progressed and suggests that the current erosion rate distribution across the island is not controlled by the initial slope spatial distribution.

5.2. Topographic control on erosion rates and influence of inherited topography

It is well recognized that, in addition to climate, topographic gradient is a first-order control on erosion (Dadson et al., 2003). Using the 25 m DEM of the present morphology of Reunion and our reconstructed paleosurfaces, we computed the basin-averaged paleo- and modern slopes as well as the paleo- and modern distribution of hillslope angles for each of the 7 studied basins. Despite the very important standard deviations ($1\sigma \gg 50\%$, not reported on figure), Fig. 5 shows a positive correlation between long-term erosion rates and present-day slopes in favor of a topographic control on erosion rates in Reunion. Yet, our paleotopography reconstructions show that the initial slopes were similar across the studied basins (Fig. 5). Because topographic gradients also evolve as erosion progresses, it indicates that the correlation in Fig. 5 may not reflect the primary control of topographic gradients in the pattern of erosion since ~70 ka. This is confirmed by the paleo- and modern distribution of the hillslope angles (Figs. S5a, S5b). In each of the reconstructed basins the hillslope angle paleodistribution shows a main mode just below 10 degrees (corresponding to the mean angle of the volcano) and another mode at a threshold angle of ~50 degrees corresponding to the steep scarps of the paleocirques. In the present-day slopes' distributions, the pattern is reversed, showing that the hillslopes steepened toward the threshold angle in every basin as the erosion progressed. With such topographic features (very steep hillslope angles) and under the tropical climate of Reunion (precipitation affecting slope stability), landsliding is expected to be a key process in the erosion of the island.

Inherited topographies, geometry and structures also influence erosion by impacting hydrological flux. Reunion Island experienced the competitive effect of edification due to lava flow accumulation and dismantling during long-lasting volcanic lulls and discrete collapses (Gillot et al., 1994; Michon et al., 2016; Oehler et al., 2008; Salvany et al., 2012). In such an evolution, the lateral boundaries of flank landslides and the limits between both volcanoes (Fig. 1a) may have facilitated incision and valley formation. Most of these resulting valleys were partly or totally filled by subsequent lava flow inundations, leaving inherited structures that would promote subsequent incision and erosion. In addition to such inherited depression topography, the studied watersheds are also associated with paleovalley structures (mapped from field observations Fig. 1a), linked to ancient boundaries of flank collapse or to the junction between the volcanoes (Fig. 1a). This combination of topographic and geological features evidently prelocated erosion in the preexisting basins. However, from equivalent initial topographic conditions (depression topography, paleovalley structure and similar paleoslopes) the 7 studied watersheds present different degrees of erosion. Inherited structure and topographies may undoubtedly explain the location of erosion on the studied watersheds but it may not be the cause of the observed difference in erosion intensities.

5.3. Effect of precipitation variability on long-term erosion

It has long been hypothesized that variations in rainfall frequency and intensity could impact rates and processes of landscape evolution (e.g. Leopold, 1951). Rainfall variability is intrinsically dependent on both the frequency of extreme precipitation events and the level of background precipitation regimes. Such variability can be quantified by calculating the coefficient of variation of daily precipitation, CV-p (and the annual coefficient of variation of daily precipitation for each year, annual CV-p). CV-p and annual CV-p (for the period 1981–2010) at each rain gauge station location show great disparity between the leeward and the windward sides of the island (Fig. S6a). Moreover, the difference during tropical cyclone events between the altered peaks of annual CV-p on the windward side rain gauges and the strong peaks on the leeward side rain gauges (Fig. S6a) indicates that the relative weight of extreme meteorological events is higher on the leeward side than on the windward side. This observation could result from the fact that large CV-p (or large annual CV-p) could be generated from moderate storms on a dry background rainfall rate. However, monthly mean precipitation rates analysis (Figs. S6c, S6d) show that rainfall events mainly occur during the hot season (austral summer) while the temperature inversion layer (when present) mean elevation is above the highest elevation of the island, leading to a spatial pattern of rainfall centered on summits (Fig. 4b). Such a pattern implies that both sides of the island share the same extreme precipitation events, as shown by the exceedance frequency plot in Fig. 1, and that the moderate or large storms accounting in the CV-p of the dry side also account in the CV-p of the wet side. Consequently, the difference in CV-p, or temporal rainfall variability, between the two sides of the island (Fig. 4d) results from the difference in background rainfall rates relative to storm intensities.

Here we show that the CV-p values and average erosion rates are spatially correlated ($r^2 = 0.7$; Fig. 4e) suggesting that the temporal pattern of rainfall variability is a decisive controlling factor on erosion rates. Furthermore, due to the difference in the spatial distribution of cyclonic vs. total rainfalls in Reunion (Figs. 4a, 4b), CV-p also expresses the impact of tropical storms on the background precipitation regime (Figs. 1c, S6): cyclones result in higher CV-p's on the arid leeward side and in lower CV-p's on the wet windward side of the island (Fig. 4d).

Therefore, our results suggest that extreme precipitation events are key determinants of long-term evolution of the island topography, but the correlation between erosion rates and CV-p (Fig. 4e) indicates that storms do not generate the same erosion level on both sides of the island, depending on the difference in background rainfall rates. The effect of extreme meteorological events on erosion rates is most intense where the contrast in intensity between heavy rainfall events and background precipitations is the strongest (Figs. 4 and 6a). Thus, simply correlating mean annual cyclonic precipitation with erosion rates (e.g. Fig. 4c) omits the underlying role of distinct background precipitation rates across the island. This implies that erosion processes and intensities in Reunion may be linked to extreme rainfall events and to factors that are dependent on background rainfall rates. This result demonstrates the link between precipitation variability and erosion rates, and indicates a clear influence of aridity on the effect of extreme rainfall events on erosion.

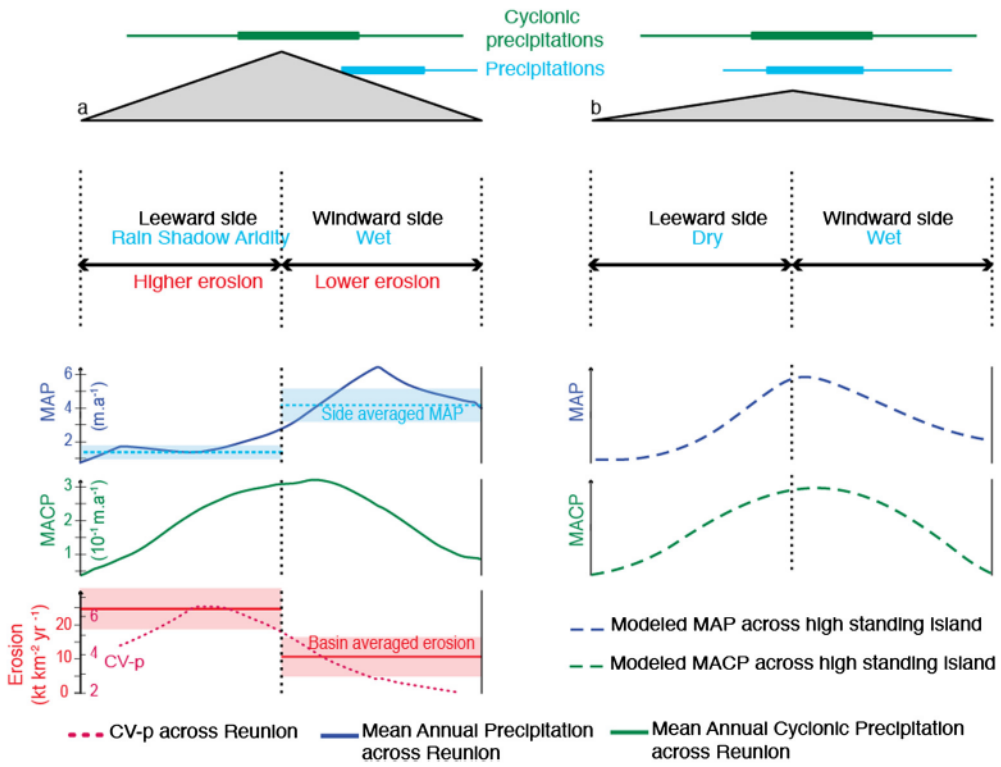

Fig. 6. Relationship between extreme precipitations, mean annual precipitations, CV-p and erosion. (**a**) Reunion island as the case study for very high standing islands. Erosion rates are the lowest in the windward side of Reunion where wet conditions buffer the effect of extreme precipitation on erosion. Erosion rates are the highest in the leeward side where rain shadow aridity establishes strong contrast between extreme precipitation events and background precipitation regime, enhancing the effect of extreme precipitation on erosion. (**b**) For high standing islands, the mean annual precipitations (MAP) and the mean annual cyclonic precipitation (MACP) are centered on the summits of the relief, obscuring the influence of both precipitation variability and extreme rainfall events on erosion.

Although modern precipitation rates may differ from paleoprecipitation rates, over the past 70 ka the spatial distribution of precipitation across Reunion has been controlled by trade winds and island topography similar to that observed today (Réchou et al., 2014; Supplementary Material). Limitation in paleoclimate data make it challenging to evaluate changes in the mean elevation of the temperature inversion layer during glacial times. Nevertheless, with similar trade winds we may infer that a lowering of the elevation of this layer during glacial periods would have enhanced the asymmetry of the Total rainfall spatial pattern, while an increase would have focused precipitation over the summits and enhanced the Cyclonic rainfall spatial pattern. Therefore, we suggest that the spatial paleopattern of the CV-p has not significantly changed over the past ~70 ka and that its correlation with erosion rates (Fig. 4e) reflects the influence of precipitation variability and extreme meteorological events on long-term erosion rates.

5.4. Implications on erosion processes and controls

Predominant processes of erosion of Reunion have undoubtedly changed over time (e.g. river incision, soil creeping, landslides, etc.). However, slope failure as a first order mechanism for erosion would be consistent with the watershed's topographic features (with hillslope angles up to ~50 degrees) and with the interpretation that precipitation variability influences erosion rates. Storm events cause landfall and debris flows in many geological settings, and influence erosion by increasing rainfall impact velocity and by mobilizing sediment into the river network (Allemand et al., 2014; Dadson et al., 2003; Reid and Page, 2003). In Reunion, such impact is evidenced by the numerous shallow to deep landslides that occur in the days following cyclonic events, providing massive amounts of sediment to the rivers (i.e. Mahavel deposit 50 × 10^6 m^3; Garcin et al., 2005), which in turn are flushed by subsequent extreme events (then enabling more river incision). Furthermore, we show an empirical relationship between long-term erosion, aridity and extreme rainfall events (Fig. 4e) implying that erosional processes in Reunion (and their efficiency) are not only linked to extreme rainfall events but also to factors related to background rainfall rates. At this stage, we speculate that background precipitation regime may play a role in modulating the efficiency of heavy rainfall events on erosion (or in restraining erosional processes), particularly through the influence of the rain on the Earth's Critical Zone. For example vegetation cover, which is primarily regulated by prevailing precipitation and temperature, improves soil strength through the densification of the root networks (Ghestem et al., 2011), and reduces soil moisture through evapotranspiration and canopy interception of precipitation. At the present time, vegetation cover can be characterized by spectral data such as enhanced vegetation index (EVI), which reflects variation in canopy structure (Huete et al., 2002), or by tree canopy cover, which distinguishes areas with high standing trees vs. other types of vegetation. Unfortunately, the effect of vegetation on long-term erosion is difficult to assess due to the complexity of former vegetation reconstructions. However, analyses of present-day EVI (averaged over 2000-2015; Modis EVI), and present-day tree canopy cover (for year 2000, tree height ≥5 m; Hansen et al., 2013) are consistent with the mean annual precipitation spatial distribution showing a slight difference in vegetation density and type between the wet windward and dry leeward side of the island. The vegetation density given by EVI (reflecting the canopy structures) is slightly higher on the windward side (0.45 vs 0.39%, Supplementary Material, Fig. S7) while the canopy closure from 5 m high trees is also in average higher in the windward side of Reunion (62% vs 50%; Supplementary Material, Fig. S7). We acknowledge that such evidence (quantitative evidence) is too weak to infer that slight differences in vegetation density and type could explain the difference in ero-

sion intensity between the two sides of the island. However, one can argue that a difference in canopy closure or vegetation density caused by the difference in background precipitation regime across Reunion, would lead to a difference in vegetation-shielding effect and thus may have influenced the erosional effect of extreme to normal rainfall between the two sides of the island. This shielding effect hypothesis is supported by the large qualitative difference in the vegetation type and distribution between the leeward dry forest and windward rainy forests (Strasberg et al., 2005). Furthermore, although Murphy et al. (2016) have shown that areas of high mean rainfall would be weakened from weathering enhancing river incision, other evidence suggests that sequentially drying and wetting of some bedrock, lithologies could dramatically decrease their strength and enhance erosion (Johnson and Finnegan, 2015). We are neither able to provide rock strength spatial distribution across the island nor rock strength after wetting and drying tests, but we suggest that such mechanisms could be considered in addition to vegetation effects and soil thickness to contribute to the higher erosion rates on the arid side of the island.

Our study shows that in Reunion the spatial variability in average long-term erosion rates can be explained by the temporal variability in precipitation rates, reflecting the differential incidence of heavy rainfall events on arid and wet environments. Such a result is possible to reach using Reunion because of a significant offset between the spatial patterns of Cyclonic and Total Precipitation Regimes. The question remains as to how broadly the influence of climate variability on long-term erosion can be constrained across other locations and settings. Volcanic islands can be divided into two groups. The "very high standing" islands, which present summits higher than the temperature inversion layer mean elevation, and the "high standing" islands, which have maximum elevation below this boundary layer mean elevation (Barcelo and Coudray, 1996; Giambelluca and Nullet, 1992; Nullet et al., 1995). Only in very high standing islands (e.g. Reunion, Hawaii, Tenerife or Fogo; Barcelo and Coudray, 1996) can a contrast between spatial patterns of Cyclonic and Total Precipitation arise (Figs. 4a, 4b and 6a). On the contrary, in high standing islands (e.g. Kauai, Guadeloupe or Gran Canaria; Barcelo and Coudray, 1996) the spatial pattern of extreme precipitation regimes would mimic that of total precipitation (Fig. 6b). Consequently, in such settings, the role of rainfall variability (e.g. Reunion vs. Kauai; Fig. S8) cannot be easily identified and the derived impact of extreme rainfall events on erosion processes is obscured by the correlation between mean annual precipitation and erosion rates. Yet, we suggest that the influence of both climate variability and extreme precipitation events on erosion can also be perceived in regions of more complex meteorological and tectonic contexts, as long as extreme precipitation maximum do not spatially coincide with maximum mean annual precipitation rates (e.g. Taiwan; Dadson et al., 2003; Su et al., 2012). However, in Reunion, the absence of major tectonic activity, the homogeneous lithology, and the offset between the spatial patterns of extreme and total precipitation give a unique opportunity to demonstrate the role and consequences of precipitation variability and extreme precipitation events on large and long-term erosion rates.

6. Conclusions

Here we used paleovolcanic reconstructions and statistical analysis of 30 years of rainfall records to show that high long-term erosion rates on Reunion Island (0.8 to ~10 mm yr^{-1} over ~70 ka) are correlated with the cyclone-driven variability of precipitation, rather than with mean annual precipitation. We show that estimated erosion rates are high where the difference in intensity between extreme rainfall and prevailing precipitation is the strongest indicating that storm control on erosion is influenced by factors that depend on background rainfall regime.

Estimation of the consequences of changes in climatic variability on landscape evolution is contingent upon specific processes and poorly constrained boundary conditions. However, our results demonstrate that climatic variability increases erosion rates and thus support the general assumption that climate shifts toward arid conditions (dominated by extreme events) may increase erosion (Molnar et al., 2006; Tucker and Bras, 2000). Furthermore, the future shifts of tropical-cyclone activity highlighted by some climatic models (e.g. Redmond et al., 2015) may expose new coastal areas (Darby et al., 2016) to high rainfall variability and erosion rates. Climatic variability is a factor that should be considered when attempting to relate climate and long-term erosion rates, not only to interpret stratigraphic records but also to predict the potential impacts of future climate changes.

Acknowledgements

We thank Météo France for their data. We thank J. Bouchez, P. Lopez, Reika Yokochi and O. Deveauchelle for discussions. We acknowledge two anonymous reviewers for their helpful comments. This work was supported by funding from INTRACRUE program (Office de l'EAU, Univeristé de la Réunion, Université de Bretagne Orientale). IPGP contribution 4033.

Funding

This work was supported by the Institut National des Sciences de l'Univers (project SYSTER), by the Intitut de Physique du Globe de Paris (programme transverse de potamologie), by the INTRACRUE project funded by the Office de l'Eau de La Réunion, the Direction de l'Environnement, de l'Aménagement et du Logement de La Réunion and the Fonds Européen de Développement Régional.

Appendix A. Supplementary material

Supplementary material related to this article can be found online at https://doi.org/10.1016/j.epsl.2019.04.003.

References

Allemand, P., Delacourt, C., Lajeunesse, E., Devauchelle, O., Beauducel, F., 2014. Erosive effects of the storm Helena (1963) on Basse Terre Island (Guadeloupe – Lesser Antilles Arc). Geomorphology 206, 79–86.

Barcelo, A., Coudray, J., 1996. Nouvelle carte des isohyètes annuelles et des maxima pluviométriques sur le massif du Piton de la Fournaise (Ile de la Réunion). Rev. Sci. Eau 9, 457–484.

Brantley, S.L., Goldhaber, M.B., Ragnarsdottir, K.V., 2007. Crossing disciplines and scales to understand the Critical Zone. Elements 3, 307–314.

Chaput, M., Famin, V., Michon, L., 2014. Deformation of basaltic shield volcanoes under cointrusive stress permutations. J. Geophys. Res., Solid Earth 119, 274–301.

Chevallier, L., Vatin-Perignon, N., 1982. Volcano-structural evolution of Piton des Neiges, Reunion Island, Indian Ocean. Bull. Volcanol. 45, 285–298.

Dadson, S., Hovius, N., Chen, H., 2003. Links between erosion, runoff variability and seismicity in the Taiwan orogen. Nature 426, 648–651.

Darby, S.E., Hackney, C.R., Leyland, J., Kummu, M., Lauri, H., Parsons, D.R., Best, J.L., Nicholas, A.P., Aalto, R., 2016. Fluvial sediment supply to a mega-delta reduced by shifting tropical-cyclone activity. Nature 539, 276–279.

DiBiase, R.A., Whipple, K.X., 2011. The influence of erosion thresholds and runoff variability on the relationships among topography, climate, and erosion rate. J. Geophys. Res. 116, F04036.

Ferrier, K.L., Huppert, K.L., Perron, J.T., 2013a. Climatic control of bedrock river incision. Nature 496, 206–209.

Ferrier, K.L., Perron, J.T., Mukhopadhyay, S., Rosener, M., Stock, J.D., Huppert, K.L., Slosberg, M., 2013b. Covariation of climate and long-term erosion rates across a steep rainfall gradient on the Hawaiian island of Kaua'i. Geol. Soc. Am. Bull. 125, 1146–1163.

Francis, P.W., Abbot, B.M., 1973. Sizes of conical volcanoes. Nature 244, 22–23.

Gallart, J., Driad, L., Charvis, P., Sapin, M., Hirn, A., Diaz, J., de Voogd, B., Sachpazi, M., 1999. Perturbation to the lithosphere along the hotspot track of La Réunion from an offshore-onshore seismic transect. J. Geophys. Res. 104, 2895–2908.
Garcin, M., Poisson, B., Pouget, R., 2005. High rates of geomorphological processes in a tropical area: the Remparts River case study (Réunion Island, Indian Ocean). Geomorphology 67, 335–350.
Gayer, E., Mukhopadhyay, S., Meade, B.J., 2008. Spatial variability of erosion rates inferred from the frequency distribution of cosmogenic ^{3}He in olivines from Hawaiian river sediments. Earth Planet. Sci. Lett. 266, 303–315.
Ghestem, M., Sidle, R.C., Stokes, A., 2011. The influence of plant root systems on subsurface flow: implications for slope stability. Bioscience 61, 869–879.
Giambelluca, T.W., Nullet, D., 1992. Evaporation at high elevations in Hawaii. J. Hydrol. 136, 219–235.
Gillot, P., Lefevre, J., Nativel, P., 1994. Model for the structural evolution of the volcanos of Reunion island. Earth Planet. Sci. Lett. 122, 291–302.
Hansen, M.C., Potapov, P.V., Moore, R., Hancher, M., Turubanova, S.A., Tyukavina, A., Thau, D., Stehman, S.V., Goetz, S.J., Loveland, T.R., Kommareddy, A., Egorov, A., Chini, L., Justice, C.O., Townshend, J.R.G., 2013. High-resolution global maps of 21st-century forest cover change. Science 342, 850–853.
Hartshorn, K., Hovius, N., Dade, W.B., Slingerland, R.L., 2002. Climate-driven bedrock incision in an active mountain belt. Science 297, 2036–2038.
Hildenbrand, A., Gillot, P.-Y., Marlin, C., 2008. Geomorphological study of long-term erosion on a tropical volcanic ocean island: Tahiti-Nui (French Polynesia). Geomorphology 93, 460–481.
Hilton, R.G., Galy, A., Hovius, N., Chen, M.-C., Horng, M.-J., Chen, H., 2008. Tropical-cyclone-driven erosion of the terrestrial biosphere from mountains. Nat. Geosci. 1, 759–762.
Huete, A., Didan, K., Miura, T., Rodriguez, E., Gao, X., Ferreira, L., 2002. Overview of the radiometric and biophysical performance of the MODIS vegetation indices. Remote Sens. Environ. 83, 195–213.
Johnson, K.N., Finnegan, N.J., 2015. A lithologic control on active meandering in bedrock channels. Geol. Soc. Am. Bull. 127, 1766–1776.
Kluska, J.M., 1997. Evolution magmatique et morpho-structurale du Piton des Neiges au cours des derniers 500 000 ans. Unpubl. PhD thesis. Université Paris Sud, pp. 93.
Larsen, I.J., Almond, P.C., Eger, A., Stone, J.O., Montgomery, D.R., Malcolm, B., 2014. Rapid soil production and weathering in the Southern Alps, New Zealand. Science 343, 637–640.
Leopold, L.B., 1951. Rainfall frequency: an aspect of climatic variation. Trans. Am. Geophys. Union 32, 347.
Louvat, P., Allègre, C.J., 1997. Present denudation rates on the island of Réunion determined by river geochemistry: basalt weathering and mass budget between chemical and mechanical erosions. Geochim. Cosmochim. Acta 61, 3645–3669.
Mairine, P., Bachèlery, P., 1997. Major erosional period in the building of Piton de la Fournaise (Reunion island). C. R. Acad. Sci. 325, 243–249.
Mazuel, A., Sisavath, E., Babonneau, N., Jorry, S., Bachelery, P., Delacourt, C., 2016. Turbidity current activity along the flanks of a volcanic edifice: the mafate volcaniclastic complex, La Réunion Island, Indian Ocean. Sediment. Geol. 335, 34–50.
Météo France, 2019. Données publiques [WWW document]. https://donneespubliques.meteofrance.fr **(accessed 1.1.15).**
Michon, L., Ferrazzini, V., DiMuro, A., Villeneuve, N., Famin, V., 2015. Rift zones and magma plumbing system of Piton de la Fournaise volcano: how do they differ from Hawaii and Etna? J. Volcanol. Geotherm. Res. 303, 112–129.
Michon, L., Lénat, J.-F., Bachèlery, P., Di Muro, A., 2016. Geology and morphostructure of Piton de la Fournaise. In: Bachèlery, P., Lénat, J.-F., Di Muro, A., Michon, L. (Eds.), Active Volcanoes of the World. Springer-Verlag, Berlin and Heidelberg, pp. 45–60.
Modis EVI, 2019. Veg. indices [WWW document]. https://modis-land.gsfc.nasa.gov/vi.html.
Molnar, P., Anderson, R.S., Kier, G., Rose, J., 2006. Relationships among probability distributions of stream discharges in floods, climate, bed load transport, and river incision. J. Geophys. Res., Earth Surf. 111, F02001.
Moon, S., Page Chamberlain, C., Blisniuk, K., Levine, N., Rood, D.H., Hilley, G.E., 2011. Climatic control of denudation in the deglaciated landscape of the Washington Cascades. Nat. Geosci. 4, 469–473.
Murphy, B.P., Johnson, J.P.L., Gasparini, N.M., Sklar, L.S., 2016. Chemical weathering as a mechanism for the climatic control of bedrock river incision. Nature 532, 223–227.
Nott, J., 2007. The importance of Quaternary records in reducing risk from tropical cyclones. Palaeogeogr. Palaeoclimatol. Palaeoecol. 251, 137–149.
Nullet, D., Juvik, J., Wall, A., 1995. A Hawaiian mountain climate cross-section. Clim. Res. 5, 131–137.
Oehler, J.-F., Lénat, J.-F., Labazuy, P., 2008. Growth and collapse of the Reunion Island volcanoes. Bull. Volcanol. 70, 717–742. https://doi.org/10.1007/s00445-007-0163-0.
Quetelard, H., Bessemoulin, P., Cerveny, R., Peterson, T., Burton, A., Boodhoo, Y., 2009. Extreme weather: world-record rainfalls during Tropical Cyclone Gamede. Bull. Am. Meteorol. Soc. 90, 603–607.
Réchou, A., Narayana Rao, T., Bousquet, O., Plu, M., Decoupes, R., 2014. Properties of rainfall in a tropical volcanic island deduced from UHF wind profiler measurements. Atmos. Meas. Tech. 7, 409–418.
Redmond, G., Hodges, K.I., Mcsweeney, C., Jones, R., Hein, D., 2015. Projected changes in tropical cyclones over Vietnam and the South China Sea using a 25 km regional climate model perturbed physics ensemble. Clim. Dyn. 45, 1983–2000.
Reid, L., Page, M., 2003. Magnitude and frequency of landsliding in a large New Zealand catchment. Geomorphology 49, 71–88.
Reiners, P.W., Ehlers, T.A., Mitchell, S.G., Montgomery, D.R., 2003. Coupled spatial variations in precipitation and long-term erosion rates across the Washington Cascades. Nature 426, 645–647.
Saint-Ange, F., Savoye, B., Michon, L., Bachelery, P., Deplus, C., De Voogd, B., Dyment, J., Le Drezen, E., Voisset, M., Le Friant, A., Boudon, G., 2011. A volcaniclastic deep-sea fan off La Reunion Island (Indian Ocean): gradualism versus catastrophism. Geology 39, 271–274.
Salvany, T., Lahitte, P., Nativel, P., Gillot, P.-Y., 2012. Geomorphic evolution of the Piton des Neiges volcano (Réunion Island, Indian Ocean): competition between volcanic construction and erosion since 1.4 Ma. Geomorphology 136, 132–147.
Sarda, P., Staudacher, T., Allègre, C.J., Lecomte, A., 1993. Cosmogenic neon and helium at Réunion: measurement of erosion rate. Earth Planet. Sci. Lett. 119, 405–417.
Scherler, D., DiBiase, R.A., Fisher, G.B., Avouac, J.-P., 2017. Testing monsoonal controls on bedrock river incision in the Himalaya and Eastern Tibet with a stochastic-threshold stream power model. J. Geophys. Res., Earth Surf. 122, 1389–1429.
Sibson, R., 1981. A brief description of natural neighbor interpolation. In: Barnett, V. (Ed.), Interpreting Multivariate Data. John Wiley, New York, pp. 21–36.
Sisavath, E., Mazuel, A., Jorry, S.J., Babonneau, N., Bachèlery, P., de Voogd, B., Salpin, M., Emmanuel, L., Beaufort, L., Toucanne, S., 2012. Processes controlling a volcaniclastic turbiditic system during the last climatic cycle: example of the Cilaos deep-sea fan, offshore La Réunion Island. Sediment. Geol. 281, 180–193.
Stallard, R.F., 1998. Terrestrial sedimentation and the carbon cycle: coupling weathering and erosion to carbon burial. Glob. Biogeochem. Cycles 12, 231–257.
Steer, P., Simoes, M., Cattin, R., Shyu, J.B.H., 2014. Erosion influences the seismicity of active thrust faults. Nat. Commun. 5.
Strasberg, D., Rouget, M., Richardson, D.M., Baret, S., Dupont, J., Cowling, R.M., 2005. An assessment of habitat diversity and transformation on La Réunion Island (Mascarene Islands, Indian Ocean) as a basis for identifying broad-scale conservation priorities. Biodivers. Conserv. 14, 3015–3032.
Su, S.-H., Kuo, H.-C., Hsu, L.-H., Yang, Y.-T., 2012. Temporal and spatial characteristics of typhoon extreme rainfall in Taiwan. J. Meteorol. Soc. Jpn. 90, 721–736.
Tucker, G.E., Bras, R.L., 2000. A stochastic approach to modeling the role of rainfall variability in drainage basin evolution. Water Resour. Res. 36, 1953–1964.
Well, A.D., Myers, J.L., 2002. Research Design & Statistical Analysis. Taylor & Francis, Oxford.
Willett, S.D., 1999. Orogeny and orography: the effects of erosion on the structure of mountain belts. J. Geophys. Res. 104, 28957–28981.